Erratum: Phonon-mediated intrinsic topological superconductivity in Fermi arcs [Phys. Rev. B 112, 104507 (2025)]

Kristian Mæland, Masoud Bahari, and Björn Trauzettel

(Received 29 July 2026; revised 5 October 2026; published 13 November 2026)

DOI: 10.1103/5l47-72d8

In the original paper, all results relying on the numerical computation of the phonon-mediated electron-electron interaction contain an error. Here, we present corrected versions of these results. The main conclusion, namely, that phonon-mediated pairing yields intrinsic topological superconductivity with a spinless chiral p-wave gap function on the surface of Weyl semimetals, remains valid. Furthermore, there is an error in Table I of the original paper regarding the phonon model. A typo in the symmetry analysis led to us setting groups of two force constants equal as enforced by symmetry. In fact, there is no symmetry argument that forces them to be equal. The original results then simply present the case where they are chosen to be equal. We present an updated version of Table I showing general force constants.

We made a point in the original paper that the phonon-mediated interaction typically prefers a local minimum of the gap magnitude in the center of the arc, unlike the prediction from a local Hubbard attraction [1]. This claim was repeated in the abstract, introduction, and conclusion. Here, we show that the typical case in fact is that a phonon-mediated attraction prefers a maximum gap magnitude in the center of the Fermi arcs. We find a new parameter set where a phonon-mediated attraction still gives a local minimum in the center of the arc. This involves introducing a dependence on the orbital degree of freedom also in the out-of-plane hopping. The mechanism behind the local minimum in the center of the Fermi arcs remains the same as stated in the original paper, but with more stringent requirements on the electronic surface states.

The motivation to focus on the local minimum of the gap in the center of the Fermi arcs was the observation of i-wave pairing in Ref. [2]. A local minimum in the gap amplitude appeared to indicate that phonon-mediated pairing might be relevant there despite the different gap symmetry. In Ref. [3], the authors show that phonon-mediated pairing combined with Coulomb repulsion can explain the i-wave gap when the surface state bandwidth is comparable to the maximum phonon energy. The mechanism also works when phonon-mediated pairing alone predicts a maximum gap magnitude in the center of the arc. The unique feature of the phonon-mediated attraction in the slab geometry, compared to a local Hubbard attraction, is that it has a long-ranged component in real space. When Coulomb repulsion then prevents short-ranged real-space Cooper pairing, the long-ranged attraction from phonons can generate higher angular momentum pairing such as the i wave. In momentum space, we identify the long-ranged component of the phonon-mediated interaction as a peak in the interaction at zero momentum transfer.

Tables I, II, and III present corrected force constants as constrained by the symmetries of the $P31m$ space group. By additionally choosing $\gamma_1 = \gamma_2$, $\rho_1 = \rho_3$, $\rho_2 = \rho_4$, $\rho_7 = \rho_9$, and $\rho_8 = \rho_{10}$, Tables I, II, and III simplify to Table I in the original paper. For the updated results presented here, we continue to choose all next-nearest-neighbor force constant parameters to be equal; $\rho_i = \rho = -\gamma_1/10\sqrt{2}$. We also set $\gamma_2 = \gamma_1$ and $\gamma_7 = \gamma_6$. Note that these choices are not enforced by symmetry, but are made for simplicity.

In the corrected results we use $Mt = 4.87 \times 10^4$ where in the original paper we used $Mt = 5.6 \times 10^4$. A lower mass slightly increases the strength of the electron-phonon coupling (EPC). $Mt = 4.87 \times 10^4$ gives $M = 204$ u (the average atomic weight in $PtBi_2$) if $t = 1$ eV and $a = 1$ Å. In the original paper we made the same claim about $Mt = 5.6 \times 10^4$ due to a typo. We stress that Figs. 1, 2, 3(f), 3(g), and 6 in the original paper remain correct as they do not rely on the electron-electron interaction.

Other than the mass, we present results with the same parameters as in the original paper in Figs. 1–4. The qualitative results are the same, but there are several quantitative changes. Figures 1 and 2 show the solution to the Fermi surface (FS) averaged linearized gap equation for the bottom surface Fermi arc. We still get a $p_x + ip_y$-wave gap and a local minimum of the gap amplitude in the center of the Fermi arc. The change is in the phonon-mediated electron-electron interaction. Unlike in the original paper, it now shows a local minimum of $\bar{V}_{\boldsymbol{k}\boldsymbol{k}'}$ at $\boldsymbol{k} = \boldsymbol{k}'$. That applies both for $\boldsymbol{k}$ in the center of the Fermi arc, and at the midpoint between the center and the end point. The local minimum in the gap amplitude in the center of the arc is due to strongest pairing when $\boldsymbol{k}$ and $\boldsymbol{k}'$ are at opposite sides of the center of the Fermi arc. That is most easily seen in Fig. 2(b).

In the original paper, we argue that $\bar{V}^{\mathrm{FS}}_{\boldsymbol{k}\boldsymbol{k}'} = -\sum_m g^m_{\boldsymbol{k}\boldsymbol{k}'} g^m_{-\boldsymbol{k},-\boldsymbol{k}'}/\omega_{\boldsymbol{k}-\boldsymbol{k}',m} + \sum_m g^m_{\boldsymbol{k},-\boldsymbol{k}'} g^m_{-\boldsymbol{k},\boldsymbol{k}'}/\omega_{\boldsymbol{k}+\boldsymbol{k}',m}$ should have a peaked absolute value at $\boldsymbol{k} = \pm\boldsymbol{k}'$ due to the out-of-plane type EPC. For that contribution, $g^m_{\boldsymbol{k}\boldsymbol{k}}$ is nonzero and $\omega_{\boldsymbol{0},m}$ is small for the optical modes. That analytic expectation still stands, so the suppression of $\bar{V}_{\boldsymbol{k}\boldsymbol{k}'}$ at $\boldsymbol{k} = \pm\boldsymbol{k}'$ in Fig. 2(b) must be due to cancellations between all the terms that contribute to the sum.

 ©2026 American Physical Society

TABLE I. Parametrization of $\Phi_{\mu\nu}(\bar{\boldsymbol{R}}_{ji})/M$ for nearest neighbors. The self-force coefficients are $\Phi_{xx}(0)/M = \Phi_{yy}(0)/M = -3\gamma_1 - 3\gamma_2 - 2\gamma_3 - 3\rho_1 - 3\rho_2 - 3\rho_3 - 3\rho_4$, $\Phi_{zz}(0)/M = -6\gamma_4 - 2\gamma_5 - 6\rho_5 - 6\rho_6$, and $\Phi_{\mu\nu}(0)/M = 0$ if $\mu \neq \nu$.

$\mu\nu$ \ $\bar{\boldsymbol{R}}_{ji}$	$\bar{\boldsymbol{\delta}}_1$	$\bar{\boldsymbol{\delta}}_2$	$\bar{\boldsymbol{\delta}}_3$	$\bar{\boldsymbol{\delta}}_4$	$\bar{\boldsymbol{\delta}}_5$	$\bar{\boldsymbol{\delta}}_6$	$\bar{\boldsymbol{\delta}}_{i=\{7,8\}}$
xx	γ_1	$-\frac{1}{2}(\gamma_1 - 3\gamma_2)$	γ_1	γ_1	$-\frac{1}{2}(\gamma_1 - 3\gamma_2)$	γ_1	γ_3
yy	γ_2	$\frac{1}{2}(3\gamma_1 - \gamma_2)$	γ_2	γ_2	$\frac{1}{2}(3\gamma_1 - \gamma_2)$	γ_2	γ_3
zz	γ_4	γ_4	γ_4	γ_4	γ_4	γ_4	γ_5
xy	$\frac{\sqrt{3}}{2}(\gamma_1 - \gamma_2)$	0	$-\frac{\sqrt{3}}{2}(\gamma_1 - \gamma_2)$	$\frac{\sqrt{3}}{2}(\gamma_1 - \gamma_2)$	0	$-\frac{\sqrt{3}}{2}(\gamma_1 - \gamma_2)$	0
yx	$\frac{\sqrt{3}}{2}(\gamma_1 - \gamma_2)$	0	$-\frac{\sqrt{3}}{2}(\gamma_1 - \gamma_2)$	$\frac{\sqrt{3}}{2}(\gamma_1 - \gamma_2)$	0	$-\frac{\sqrt{3}}{2}(\gamma_1 - \gamma_2)$	0
xz	γ_6	0	$-\gamma_6$	γ_7	0	$-\gamma_7$	0
zx	γ_7	0	$-\gamma_7$	γ_6	0	$-\gamma_6$	0
yz	$\frac{\gamma_6}{\sqrt{3}}$	$-\frac{2\gamma_7}{\sqrt{3}}$	$\frac{\gamma_6}{\sqrt{3}}$	$\frac{\gamma_7}{\sqrt{3}}$	$-\frac{2\gamma_6}{\sqrt{3}}$	$\frac{\gamma_7}{\sqrt{3}}$	0
zy	$\frac{\gamma_7}{\sqrt{3}}$	$-\frac{2\gamma_6}{\sqrt{3}}$	$\frac{\gamma_7}{\sqrt{3}}$	$\frac{\gamma_6}{\sqrt{3}}$	$-\frac{2\gamma_7}{\sqrt{3}}$	$\frac{\gamma_6}{\sqrt{3}}$	0

That is confirmed by considering Fig. 3 showing superconductivity on the top surface. There, $\bar{V}_{\boldsymbol{k}\boldsymbol{k}'}$ is peaked at $\boldsymbol{k} = \boldsymbol{k}'$, unlike the usual case for phonons. With the corrected calculation, it is now the top surface that dominates the superconductivity (has the largest T_c). We confirm that in Fig. 4 with an updated version of Fig. 4 in the original paper. Now, we see that the gap is negligible outside the top surface Fermi arc on the full FS. For the top surface, we find a maximum gap amplitude in the center of the Fermi arc. That is because the phonon-mediated attraction is strongest in the center of the arc.

We obtain that $\bar{V}_{\boldsymbol{k}\boldsymbol{k}'}$ is peaked at $\boldsymbol{k} = \boldsymbol{k}'$ on both surfaces by tuning the phonon parameters, specifically we reduce the phonon energy at $\boldsymbol{q} = 0$ and increase it at $\boldsymbol{q} = \boldsymbol{M}$ compared to the original paper. See Fig. 5(d) for the phonon spectrum at new parameters. In that case, we find that the most common behavior is to have maximum gap amplitude in the center of the Fermi arc on both surfaces.

A natural question is if it is still possible to find a local minimum of the gap in the center of the Fermi arc as presented in the original paper when $\bar{V}_{\boldsymbol{k}\boldsymbol{k}'}$ is peaked at $\boldsymbol{k} = \boldsymbol{k}'$ on both surfaces. For that, we find it necessary to introduce a separate hopping strength for intra- and interorbital hopping out of plane. We label these β and β_o, respectively. Then, the upper diagonal block in the slab Hamiltonian matrix is

$$H_U(\boldsymbol{k}) = \frac{1}{2}\begin{pmatrix} \beta & 0 & \beta_o & -s_{\boldsymbol{k}} \\ 0 & \beta & -s_{\boldsymbol{k}}^* & \beta_o \\ -\beta_o & -s_{\boldsymbol{k}} & -\beta & 0 \\ -s_{\boldsymbol{k}}^* & -\beta_o & 0 & -\beta \end{pmatrix}. \tag{1}$$

With the hierarchy of hopping amplitudes $|t_o| < |\beta_o| < t < \beta$, we find a local minimum of the gap in the center of the Fermi arc in Fig. 6(a). From Fig. 6(b) we see that the reason is that here, the phonon-mediated attraction $\bar{V}_{\boldsymbol{k}\boldsymbol{k}}$ is weaker in the center of the arc than at the midpoint between the center and the end point of the arc. The new electron bands and full FS are shown in Figs. 5(a) and 5(c). Note that compared to the parameters used in the original paper, the surface states are less extremely surface localized [compare Fig. 1(c) in the original paper and Fig. 5(c)]. Also, the two surface states that cross between $\boldsymbol{\Gamma}$ and

TABLE II. Parametrization of $\Phi_{\mu\nu}(\bar{\boldsymbol{R}}_{ji})/M$ for the next-nearest neighbors in the positive z direction.

$\mu\nu$ \ $\bar{\boldsymbol{R}}_{ji}$	$\bar{\boldsymbol{\tau}}_1$	$\bar{\boldsymbol{\tau}}_2$	$\bar{\boldsymbol{\tau}}_3$	$\bar{\boldsymbol{\tau}}_4$	$\bar{\boldsymbol{\tau}}_5$	$\bar{\boldsymbol{\tau}}_6$
xx	ρ_1	$-\frac{1}{2}(\rho_2 - 3\rho_4)$	ρ_1	ρ_2	$-\frac{1}{2}(\rho_1 - 3\rho_3)$	ρ_2
yy	ρ_3	$\frac{1}{2}(3\rho_2 - \rho_4)$	ρ_3	ρ_4	$\frac{1}{2}(3\rho_1 - \rho_3)$	ρ_4
zz	ρ_5	ρ_6	ρ_5	ρ_6	ρ_5	ρ_6
xy	$\frac{\sqrt{3}}{2}(\rho_1 - \rho_3)$	0	$-\frac{\sqrt{3}}{2}(\rho_1 - \rho_3)$	$\frac{\sqrt{3}}{2}(\rho_2 - \rho_4)$	0	$-\frac{\sqrt{3}}{2}(\rho_2 - \rho_4)$
yx	$\frac{\sqrt{3}}{2}(\rho_1 - \rho_3)$	0	$-\frac{\sqrt{3}}{2}(\rho_1 - \rho_3)$	$\frac{\sqrt{3}}{2}(\rho_2 - \rho_4)$	0	$-\frac{\sqrt{3}}{2}(\rho_2 - \rho_4)$
xz	ρ_7	0	$-\rho_7$	ρ_{10}	0	$-\rho_{10}$
zx	ρ_9	0	$-\rho_9$	ρ_8	0	$-\rho_8$
yz	$\frac{\rho_7}{\sqrt{3}}$	$-\frac{2\rho_{10}}{\sqrt{3}}$	$\frac{\rho_7}{\sqrt{3}}$	$\frac{\rho_{10}}{\sqrt{3}}$	$-\frac{2\rho_7}{\sqrt{3}}$	$\frac{\rho_{10}}{\sqrt{3}}$
zy	$\frac{\rho_9}{\sqrt{3}}$	$-\frac{2\rho_8}{\sqrt{3}}$	$\frac{\rho_9}{\sqrt{3}}$	$\frac{\rho_8}{\sqrt{3}}$	$-\frac{2\rho_9}{\sqrt{3}}$	$\frac{\rho_8}{\sqrt{3}}$

TABLE III. Parametrization of $\Phi_{\mu\nu}(\bar{\boldsymbol{R}}_{ji})/M$ for the next-nearest neighbors in the negative z direction.

$\mu\nu$ \ $\bar{\boldsymbol{R}}_{ji}$	$\bar{\boldsymbol{\tau}}_7$	$\bar{\boldsymbol{\tau}}_8$	$\bar{\boldsymbol{\tau}}_9$	$\bar{\boldsymbol{\tau}}_{10}$	$\bar{\boldsymbol{\tau}}_{11}$	$\bar{\boldsymbol{\tau}}_{12}$
xx	ρ_2	$-\frac{1}{2}(\rho_1-3\rho_3)$	ρ_2	ρ_1	$-\frac{1}{2}(\rho_2-3\rho_4)$	ρ_1
yy	ρ_4	$\frac{1}{2}(3\rho_1-\rho_3)$	ρ_4	ρ_3	$\frac{1}{2}(3\rho_2-\rho_4)$	ρ_3
zz	ρ_6	ρ_5	ρ_6	ρ_5	ρ_6	ρ_5
xy	$\frac{\sqrt{3}}{2}(\rho_2-\rho_4)$	0	$-\frac{\sqrt{3}}{2}(\rho_2-\rho_4)$	$\frac{\sqrt{3}}{2}(\rho_1-\rho_3)$	0	$-\frac{\sqrt{3}}{2}(\rho_1-\rho_3)$
yx	$\frac{\sqrt{3}}{2}(\rho_2-\rho_4)$	0	$-\frac{\sqrt{3}}{2}(\rho_2-\rho_4)$	$\frac{\sqrt{3}}{2}(\rho_1-\rho_3)$	0	$-\frac{\sqrt{3}}{2}(\rho_1-\rho_3)$
xz	ρ_8	0	$-\rho_8$	ρ_9	0	$-\rho_9$
zx	ρ_{10}	0	$-\rho_{10}$	ρ_7	0	$-\rho_7$
yz	$\frac{\rho_8}{\sqrt{3}}$	$-\frac{2\rho_9}{\sqrt{3}}$	$\frac{\rho_8}{\sqrt{3}}$	$\frac{\rho_9}{\sqrt{3}}$	$-\frac{2\rho_8}{\sqrt{3}}$	$\frac{\rho_9}{\sqrt{3}}$
zy	$\frac{\rho_{10}}{\sqrt{3}}$	$-\frac{2\rho_7}{\sqrt{3}}$	$\frac{\rho_{10}}{\sqrt{3}}$	$\frac{\rho_7}{\sqrt{3}}$	$-\frac{2\rho_{10}}{\sqrt{3}}$	$\frac{\rho_7}{\sqrt{3}}$

$\boldsymbol{M}$ in Fig. 5(a) seem to show some degree of hybridization. In other words, there are finite-size effects, unlike the case at the parameters used in the original paper.

Remember that the weight of the states is defined as $W_{\boldsymbol{k}n} = \sum_{z_i=1}^{L}(z_i-1)|\psi_{\boldsymbol{k}n,z_i}|^2/(L-1)$, where $|\psi_{\boldsymbol{k}n,z_i}|^2$ is the sum of squares of the four entries in the eigenvector of band n associated with layer z_i. By considering $|\psi_{\boldsymbol{k}n,z_i}|^2$ for the bands with Fermi arcs and with momentum in the center of the Fermi arc, we find that as a function of z_i, $|\psi_{\boldsymbol{k}n,z_i}|^2$ shows a smooth exponential decay from the surface at the parameters in Fig. 1. The occupation on the layer next to the surface is not negligible, and so the out-of-plane contribution to EPC is not suppressed in the center of the Fermi arc. At the parameters used in Fig. 5, on the other hand, $|\psi_{\boldsymbol{k}n,z_i}|^2$ shows a jagged behavior. The electrons are spread on more layers close to the surface, but at the same time certain layers have a very small, almost negligible occupation compared to their neighbors. We conjecture that this suppresses the contribution from the out-of-plane type EPC in the center of the arc. As the momentum moves along the arc, the occupation on the previously suppressed layers increases, and so does the strength of EPC. Eventually, when approaching the end of the Fermi arc the states become more bulklike, and then the strength of the phonon-mediated electron-electron attraction decreases again. Jagged occupation on layers could be the case in $PtBi_2$ due to its trilayer structure [4,5]. A jagged occupation on layers can also occur in other Weyl semimetals, an example being the diamond lattice model in Ref. [6].

Additionally, we note that the hopping hierarchy $|t_o| < |\beta_o| < t < \beta$ could be reasonable for $PtBi_2$. The orbitals in the effective model are unspecified, but the signs of hoppings indicate that one has even and the other has odd parity. In $PtBi_2$,

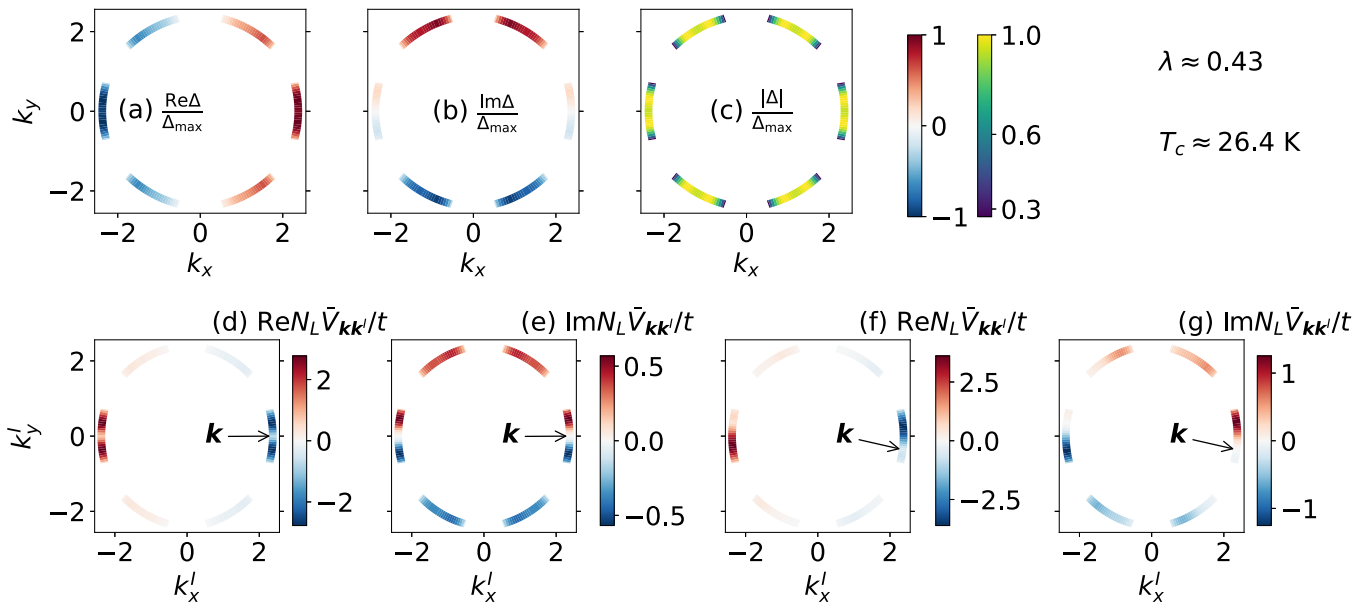


FIG. 1. (a) Real, (b) imaginary, and (c) absolute value of the gap function on the bottom surface Fermi arc. The values are scaled by the maximum absolute value of the gap $\Delta_{\max}$. The absolute value of the gap is the same on all six arcs. (d)–(g) give the phonon-mediated electron-electron interaction $\bar{V}_{\boldsymbol{k}\boldsymbol{k}'}$ as a function of $\boldsymbol{k}'$ with $\boldsymbol{k}$ fixed as indicated. The parameters are $t_o/t = 1.5$, $\beta/t = -1.5$, $\mu/t = -0.05$, $\mu_o/t = 0.2$, $\alpha/t = -0.18$, $\gamma/t = -0.2$, $\gamma_1 = -(0.005t)^2$, $\gamma_3 = \gamma_5 = 0.45\gamma_1$, $\gamma_4 = \gamma_1$, $\gamma_6 = 1.5\gamma_1$, $M = 4.87 \times 10^4/t$, $\chi = 8$, $N_{\text{samp}} = 150$, and $L = 40$.

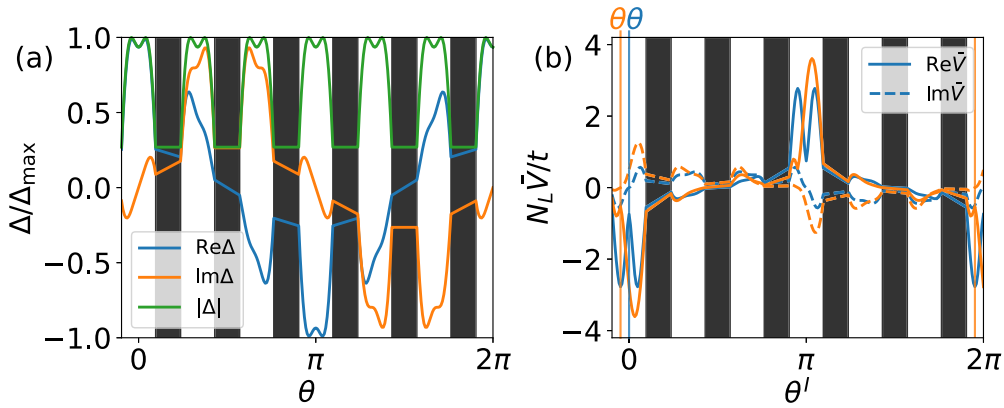


FIG. 2. (a) The same as Figs. 1(a)–1(c), but now shown as a function of the angle θ that $\boldsymbol{k}$ makes with the k_x axis. The black regions indicate directions where there is no Fermi arc. Here, we do not solve for the gap, and so the lines are just linearly interpolated. We show a bit more than one full revolution. (b) The phonon-mediated electron-electron interaction $\bar{V}_{\boldsymbol{k}\boldsymbol{k}'}$ as a function of the azimuthal angle θ' of $\boldsymbol{k}'$. The azimuthal angle θ for $\boldsymbol{k}$ is fixed as indicated for the blue and orange curves; in the center of a Fermi arc and the midpoint between the center and end point, respectively. The parameters are the same as Fig. 1.

p- and d-wave orbitals dominate [5]. Thus, it seems reasonable that interorbital hopping is smaller than intraorbital hopping. In general, for multiorbital systems, $\beta_o = \beta$ is less likely than $\beta_o \neq \beta$, so this change of the model is more realistic.

With calculations such as Ref. [3], we briefly consider the role of Coulomb repulsion for the case of a large surface state bandwidth compared to the maximum phonon energy. If EPC prefers a local minimum of the gap at the center of the Fermi arcs, adding Coulomb repulsion decreases the gap amplitude there relative to the gap maximum. That is because the Coulomb repulsion is strongest in the center of the Fermi arcs.

Finally, Eqs. (B1) and (B2) in the original paper should read

$$V = \sum_{i\alpha\neq j\beta} V(\bar{\boldsymbol{r}}_{j\beta} - \bar{\boldsymbol{r}}_{i\alpha}) \approx \sum_{i\alpha\neq j\beta} \left[V(\bar{\boldsymbol{R}}_{j\beta} - \bar{\boldsymbol{R}}_{i\alpha}) + \sum_{\mu}(V) r_{i\alpha\mu}\Big|_{\text{eq}} u_{i\alpha\mu} + \frac{1}{2}\sum_{\mu\nu} \frac{\partial^2 V}{\partial r_{i\alpha\mu}\partial r_{j\beta\nu}}\Big|_{\text{eq}} u_{i\alpha\mu}u_{j\beta\nu} \right], \tag{2}$$

$$V = \frac{1}{2}\sum_{i\alpha\mu,\,j\beta\nu} \frac{\partial^2 V}{\partial r_{i\alpha\mu}\partial r_{j\beta\nu}}\Big|_{\text{eq}} u_{i\alpha\mu}u_{j\beta\nu} = \frac{1}{2}\sum_{i\alpha\mu,\,j\beta\nu} \Phi^{\alpha\beta}_{\mu\nu}(\bar{\boldsymbol{R}}_j - \bar{\boldsymbol{R}}_i) u_{i\alpha\mu}u_{j\beta\nu}, \tag{3}$$

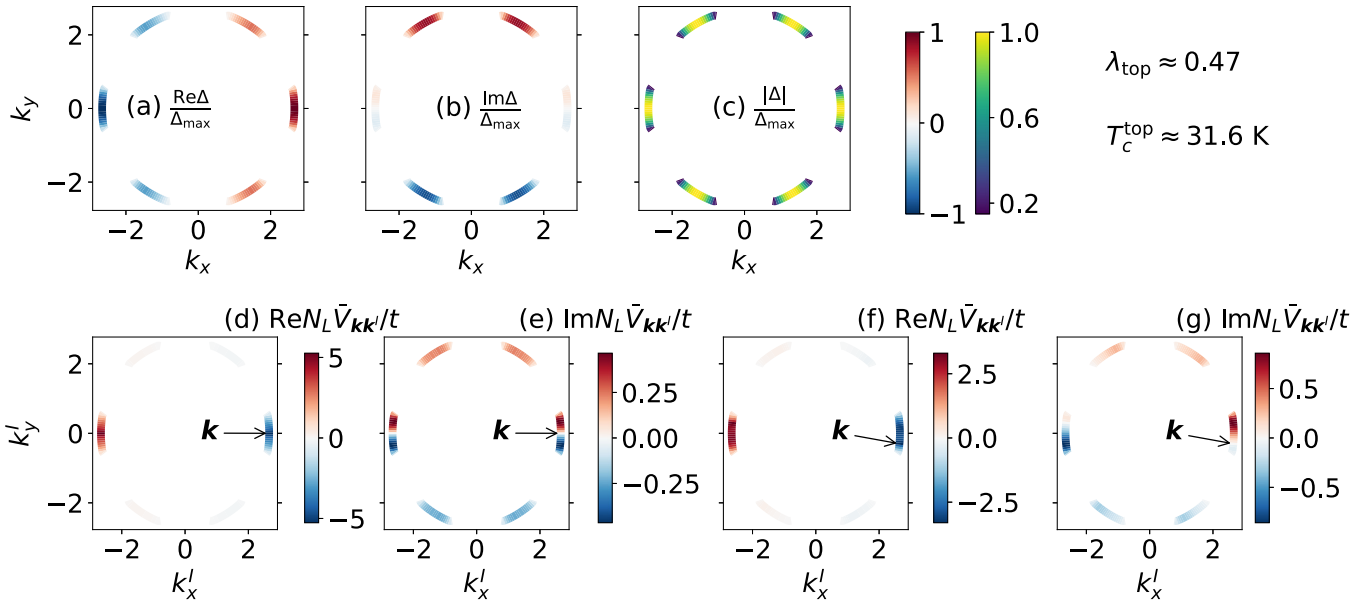


FIG. 3. (a) Real, (b) imaginary, and (c) absolute value of the gap function on the top surface Fermi arc. The values are scaled by the maximum absolute value of the gap Δ_{max}. The absolute value of the gap is the same on all six arcs. (d)–(g) give the electron-electron coupling $\bar{V}_{\boldsymbol{k}\boldsymbol{k}'}$ as a function of $\boldsymbol{k}'$ with $\boldsymbol{k}$ fixed as indicated. The parameters are $N_{\text{samp}} = 126$ and otherwise the same as Fig. 1.

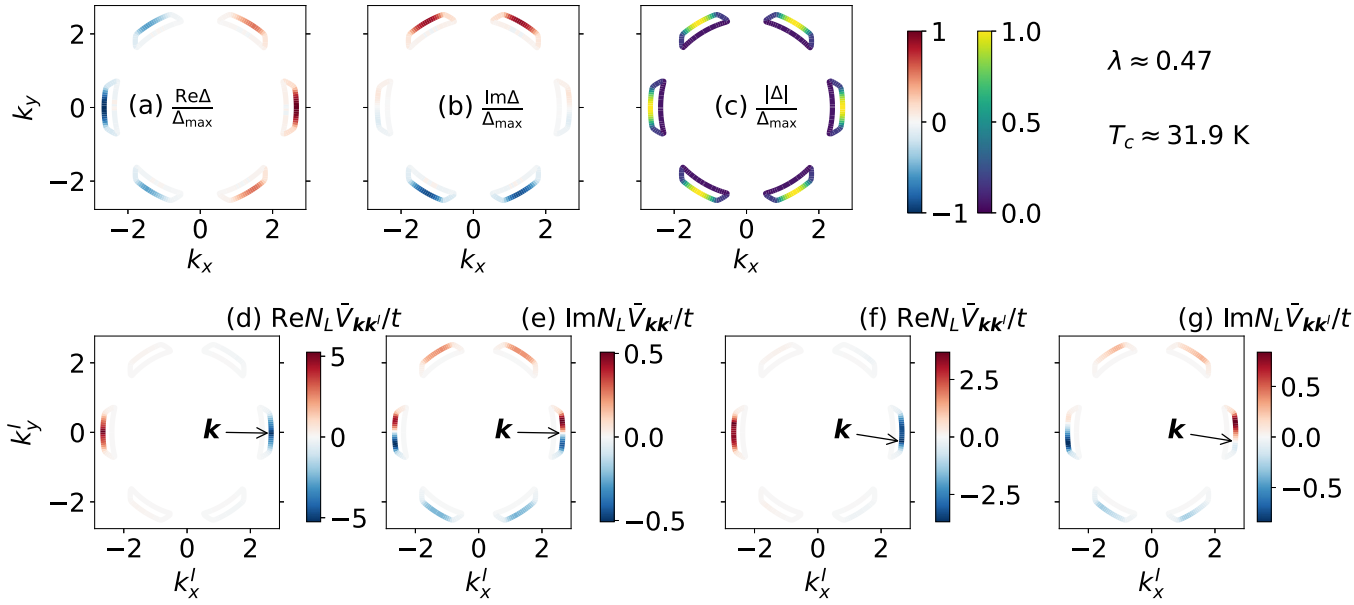


FIG. 4. (a) Real, (b) imaginary, and (c) absolute value of the gap function on the full Fermi surface (FS). The values are scaled by the maximum absolute value of the gap $\Delta_{\max}$. The absolute value of the gap is the same on all six pockets. (d)–(g) give the electron-electron coupling $\bar{V}_{\boldsymbol{k}\boldsymbol{k}'}$ as a function of $\boldsymbol{k}'$ with $\boldsymbol{k}$ fixed as indicated. The parameters are $N_{\text{samp}} = 330$ and otherwise the same as Fig. 1.

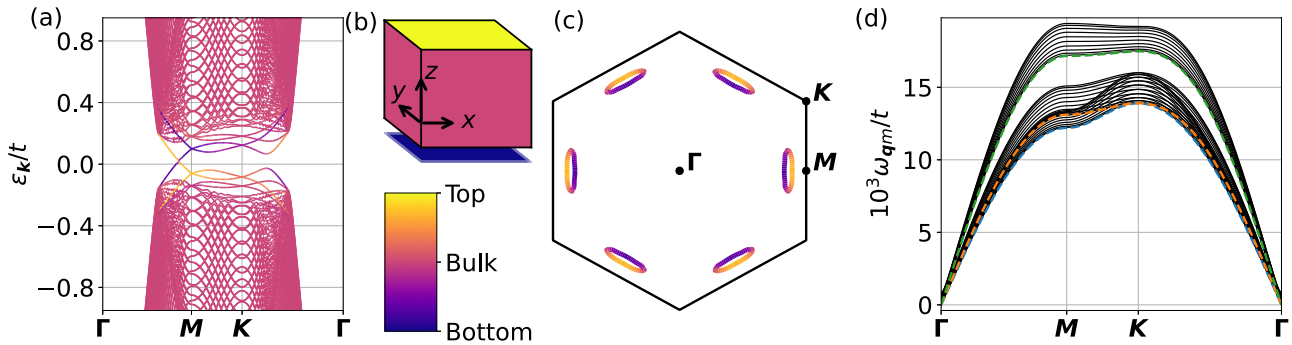


FIG. 5. (a) Electron bands in a slab geometry, with each band colored by the weight of its eigenstate W_{kn}. (b) Illustration of the system and the color code for top surface, bulk, and bottom surface. (c) FS shown within the first Brillouin zone, colored by the weight of the eigenstate. The full FS contains the Fermi arcs on the two surfaces and the projection of the bulk FS. (d) Black lines show the phonon spectrum in a slab geometry. Blue, orange, and green dashed lines show the three acoustic phonon modes with periodic boundary conditions in all directions at $q_z = 0$. The parameters are $t_o/t = 0.05$, $\beta/t = -1.5$, $\beta_o/t = -0.1$, $\mu/t = -0.02$, $\mu_o/t = -1.3$, $\alpha/t = -0.08$, $\gamma/t = -0.08$, $\gamma_1 = -(0.005t)^2$, $\gamma_3 = 0.43\gamma_1$, $\gamma_4 = 1.5\gamma_1$, $\gamma_5 = 0.432\gamma_1$, $\gamma_6 = 0.6\gamma_1$, (a), (c) $L = 45$, and (d) $L = 10$.

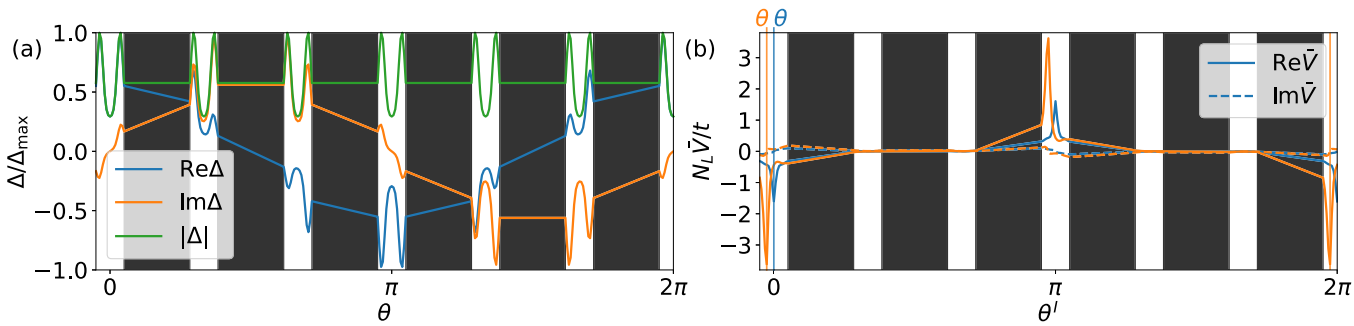


FIG. 6. (a) Real, imaginary, and absolute value of the gap function on the bottom surface Fermi arc, which dominates the superconductivity at the new parameters. The gaps are shown as a function of the angle θ that $\boldsymbol{k}$ makes with the k_x axis, still giving us a $p_x + ip_y$-wave gap function in the band basis. The black regions indicate directions where there is no Fermi arc. (b) The phonon-mediated electron-electron interaction $\bar{V}_{\boldsymbol{k}\boldsymbol{k}'}$ as a function of the azimuthal angle θ' of $\boldsymbol{k}'$. The azimuthal angle θ for $\boldsymbol{k}$ is fixed as indicated for the blue and orange curves; in the center of a Fermi arc and the midpoint between the center and end point, respectively. The parameters are $M = 4.87 \times 10^4/t$, $\chi = 14$, $N_{\text{samp}} = 102$, $L = 45$, and otherwise the same as Fig. 5. We find $\lambda \approx 0.34$ giving $T_c \approx 13.7$ K if $t = 1$ eV.

i.e., while the derivatives are evaluated in equilibrium, the derivatives of $V(\bar{\boldsymbol{r}}_{j\beta} - \bar{\boldsymbol{r}}_{i\alpha})$ should be taken with respect to the instantaneous positions $\bar{\boldsymbol{r}}_{i\alpha}$ and $\bar{\boldsymbol{r}}_{j\beta}$. These typos had no consequence as we did not model the potential energy $V(\bar{\boldsymbol{r}}_{j\beta} - \bar{\boldsymbol{r}}_{i\alpha})$ nor compute these derivatives to derive the phonon spectrum.

We thank Kristoffer Leraand for pointing out the error in our original calculation.

---

[1] M. Trama, V. Könye, I. C. Fulga, and J. van den Brink, Self-consistent surface superconductivity in time-reversal symmetric Weyl semimetals, Phys. Rev. B **112**, 064514 (2025).

[2] S. Changdar, O. Suvorov, A. Kuibarov, S. Thirupathaiah, G. Shipunov, S. Aswartham, S. Wurmehl, I. Kovalchuk, K. Koepernik, C. Timm, B. Büchner, I. C. Fulga, S. Borisenko, and J. van den Brink, Topological nodal *i*-wave superconductivity in $PtBi_2$, Nature (London) **647**, 613 (2025).

[3] K. Mæland, G. Sangiovanni, and B. Trauzettel, Mechanism for nodal topological superconductivity on $PtBi_2$ surface, Phys. Rev. Lett. **137**, 056001 (2026).

[4] G. Shipunov, I. Kovalchuk, B. R. Piening, V. Labracherie, A. Veyrat, D. Wolf, A. Lubk, S. Subakti, R. Giraud, J. Dufouleur, S. Shokri, F. Caglieris, C. Hess, D. V. Efremov, B. Büchner, and S. Aswartham, Polymorphic $PtBi_2$: Growth, structure, and superconducting properties, Phys. Rev. Mater. **4**, 124202 (2020).

[5] R. Vocaturo, K. Koepernik, J. I. Facio, C. Timm, I. C. Fulga, O. Janson, and J. van den Brink, Electronic structure of the surface-superconducting Weyl semimetal $PtBi_2$, Phys. Rev. B **110**, 054504 (2024).

[6] R. Okugawa and S. Murakami, Dispersion of Fermi arcs in Weyl semimetals and their evolutions to Dirac cones, Phys. Rev. B **89**, 235315 (2014).